Zeeman Effect in Mercury

Dennis V. Perepelitsa*
MIT Department of Physics
(Dated: May 17, 2007)

Using a Fabry-Perot interferometer, we investigate hyperfine effects and the Zeeman effect in the green line and yellow doublet of mercury. Hyperfine structure and Zeeman splitting is confirmed in the green line. The electron charge to mass ratio is calculated at $e/m = 1.82(4) \times 10^{11}$ C/kg. We fail to confirm Zeeman splitting in the yellow doublet.

1. INTRODUCTION

Michael Faraday first examined atomic spectra under the influence of a magnetic field in 1862 without much success. It would prove to be his final experimental attempt. Upon discovery of this fact, Pieter Zeeman again attempted the procedure in 1896, and was led to the startling conclusion that spectral lines seemed to split into multiple components in the presence of a magnetic field. Known as the *Zeeman effect*, this phenomenon predicted the existence of the electron before a theory of it was first published a year later.

Zeeman went on to win the Nobel Prize in Physics in 1902 for his work. The effect that is his namesake has a natural quantum mechanical description and is easily observable with modern equipment. In this paper, we describe and verify this in mercury.

2. THEORY

2.1. Zeeman Effect

In the presence of the magnetic field B, the Hamiltonian for an electron of charge e and mass m_e gains an additional field-dependent term. We can take the field to lie in the direction of the angular momentum vector $\hat{z}$. This component $\hat{H}$ breaks the degeneracy of the energy levels according to the quantum number m_j, the total angular momentum. The energy corrections $E_z(j)$ are

$$\hat{H}_z = \frac{eB}{2m_e}\left(\vec{L} + 2\vec{S}\right), \quad E_z(j) = \frac{\hbar eB}{2m_e} g m_j \tag{1}$$

The quantity g is known as the *Lange g-factor*, and is well-approximated by

$$g \approx 1 + \frac{j(j+1) + s(s+1) - l(l+1)}{2j(j+1)} \tag{2}$$

In general, a transition between states a and b with g-factors g_a and g_b and total angular momentum m_a and m_b, respectively, exhibits an energy offset $(m_b g_b - m_a g_a)\frac{\hbar eB}{2m_e}$. Every transition of this form with $\Delta m_j = 0, \pm 1$, as required by selection rules, occurs. In this experiment, we are interested in the 5460Å singlet and the 5770Å and 5790Å doublet transitions in mercury. The electronic configuration of mercury gives insight into the quantum numbers associated with any energy level. The fourth and fifth energy levels are completely filled through the $4d$ and $5f$ orbitals, respectively. Thus, in many ways, mercury behaves like a simpler, Bohric, atom. The two outer valence electrons mean that the spin is always $S = 1$.

2.2. Hyperfine Splitting

Even in the absence of a magnetic field, many spectral lines exhibits a hyperfine structure due to the isotope effects. Two relatively small effects which are present in all isotopes are small corrections to the energy due the changes in the mass and volume of the nucleus. The most pronounced effect, however, is due to the addition of nuclear spin. In an odd-numbered isotope, the nucleus itself has some intrinsic spin I. Just as the total angular momentum J was introduced to couple the effects of L and S, a new quantity $F = I + J$ called the *coupled angular momentum* must now be introduced. The transition lines for odd-numbered isotopes will split along values of this new observable.

2.3. Fabry-Perot Interferometer

The heart of a Fabry-Perot apparatus consists of two parallel reflective mirrors, diagrammed in Figure 1. For light to interfere constructively (that is, two parallel rays are in phase) as it exits the second mirror, the distance traveled $2D\cos\alpha$ must be an integer multiple of the wavelength $m\lambda$. Light of this wavelength will cause bright, concentric interference fringes to appear on the focal plane of the apparatus. m is known as the *order of interference*. Lower orders appear as brighter rings, since the mirrors are not perfectly reflective.

Evidently, the change in plate separation δD required to move the interference pattern by a fractional wavelength $\delta\lambda$ is

*Electronic address: dvp@mit.edu

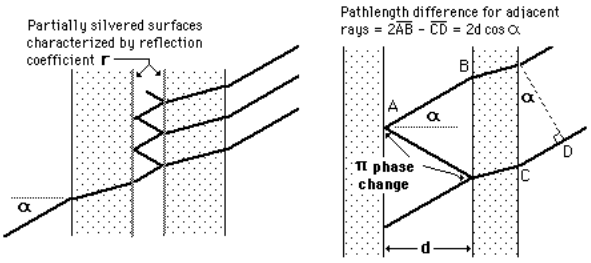

FIG. 1: Schematic of Fabry-Perot apparatus geometry, with incident angle α, wavelength λ and plate separation D. Taken from [1].

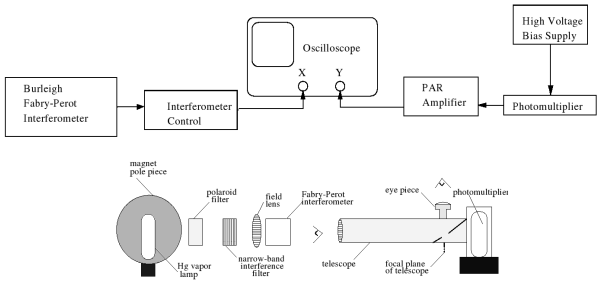

FIG. 2: The aligned experimental setup. Modified from the laboratory guide [2].

$$\delta D = m\delta\lambda/2D\cos\alpha, \tag{3}$$

and the change in plate separation ΔD required to move the interference pattern by an entire order is

$$\Delta D = \lambda/2D\cos\alpha \tag{4}$$

Assuming that the incident angle is close enough to 0 such that the small-angle approximation can be used, we can combine Equations 3 and 4 to express the change in wavenumber (reciprocal wavelength) between any two points in the observed interference pattern entirely in terms of the ratio of changes in the plate separations.

$$\Delta\left(\frac{1}{\lambda}\right) = \frac{1}{2D}\frac{\delta D}{\Delta D} \tag{5}$$

Through the relation of frequency to energy, Equation 5 is the mechanism by which emission spectra are calibrated.

3. EXPERIMENTAL SETUP

Our setup is pictured in Figure 2. A low-pressure mercury lamp is situated inside a variable-current electromagnet. Radiation passes through a narrow-band interference filter centered around the desired wavelength, and enters the Fabry-Perot interferometer. This device consists of two reflective parallel plates which serve to transmit strong incoming radiation at different orders of wavelength. The apparatus has a built-in minimum separation $D = 12.212(15)$ mm, obtained via collaborative measurement with the laboratory staff, which is the *measured* separation at which the plates meet. Small knobs allow careful adjustment of the plate separation to high accuracy.

Multiple orders of the interference pattern appear as concentric rings in the focal plane of the aligned telescope, and a mirror at angle of 45% allows the pattern can be investigated with the naked eye. A small aperture in the middle of the pattern leads to an adjacent photomultiplier tube, which measures the intensity of incident radiation. This signal is amplified and filtered, and is connected to an oscilloscope input.

During a spectrum scan, the interferometer control changes the alignment of the plates by applying a sawtooth function of voltage to small piezoelectric crystals controlling the plate separation. The interference pattern is observed to sweep inward and outward across the aperture as the voltage rises and falls. An interface on the ramp control system allows the experimenter to determine the height, length and slope of the ramp. The voltage output is also connected to an oscilloscope input. In this way, the system obtains a high-resolution scan over a narrow band of frequencies.

At the beginning of each day, we aligned the apparatus to maximize the intensity of the lines in question.

4. ERROR ANALYSIS

Our results included an investigation of sources of error at several levels of analysis.

Fundamentally, every digitized spectrum exhibited a certain voltage granularity, on the order of 1%. Background fluctuations in the signal were either too low to be noticed within this signal granularity, or unable to be estimated from the available data, and were not figured into calculations. Though atomic emission is a Poisson process, we do did not model this or attempt to investigate the raw counts in the photomultiplier tube, because even a modest number of counts would serve to make the relative uncertainty less than voltage granularity.

In every case, the voltage ramp was linear to the point that time could be used as a proxy variable with no loss of precision. When measuring the energy difference between two peaks δD as calibrated by the separation of different orders ΔD we propagated the error in the fitted parameters of profile centers. The uncertainty in the wavenumber was the uncertainty in each of these quantities added in quadrature, as required by Equation 5. While collecting data on the green line, the uncertainty in D could be ignored, but became a significant source of

error during the higher free spectral range of the yellow doublet.

When peak energy separation was plotted against field strength, the uncertainty of the magnetic field, which was about 1%, was added in quadrature to the data. After linear fits were obtained, the final value of e/m was derived by taking a weighted average of the best-fit slopes, as described in [3].

The exception to the above analysis is our treatment of the hyperfine spectrum of the green line. In this case, fitting proved impossible, and we took the highest point of each peak to be the center, and assigned the granularity in the x-axis as the uncertainty.

5. RESULTS

Using the setup outlined above, we investigated the green and yellow lines of mercury. The mirror separation D was 14.00(5) mm and 12.35(5) mm, respectively, for the two lines. This allowed for a free spectral range $\Delta\lambda$ large enough to use adjacent orders for an energy calibration, but small enough to resolve the Zeeman splitting within the lines. The range of values of magnetic field B lay between the value produced by the maximum safe current (about 10.7 kG) to the lowest value at which Zeeman splitting was still distinguishable (about 6 kG for the green line).

Since the response of the magnetic field to current is not linear, the samples are biased towards higher magnetic fields. To determine the uncertainty in the magnetic field, several spatial points within the electromagnet were sampled with a calibrated Gaussmeter probe.

All of the spectra below have been fitted with variable-width Lorentzian profiles. This was motivated by observing better values of the reduced chi squared parameter for Lorentzian profile fits than Gaussian ones on sample spectra. The legitimacy of this approach will be discussed later. The reduced-chi-squared values were in the lower single digits, reflecting the imprecision in this choice of model.

5.1. Hyperfine Splitting in 5460Å

The hyperfine spectrum of the green line is shown in Figure 3. Evidently, the dominant, wide central peak consists of unresolved transition lines of the even isotopes of mercury, the most abundant of these being ^{200}Hg and ^{202}Hg. There are two other identifiable peaks - at $-.351(8)$ cm^{-1} and .860(8) cm^{-1}, respectively. The most probable identity of these peaks are the nuclear-spin split transition lines of the abundant, stable isotope ^{199}Hg. [4] gives the accepted values of these as $-.315$ cm^{-1} and .753 cm^{-1}, respectively.

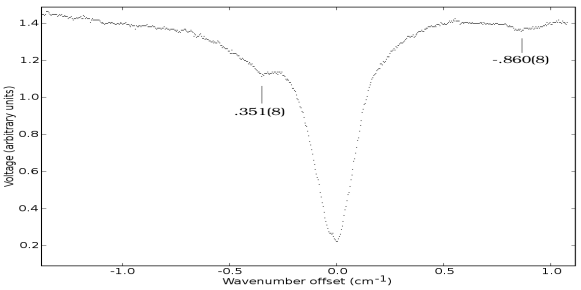

FIG. 3: Spectrum of the green line of mercury in the absence of a magnetic field. Hyperfine structure is barely resolvable.

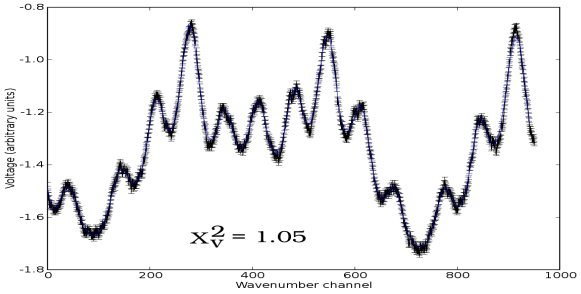

FIG. 4: The nine Zeeman peaks of the green line of mercury at 10.7 kG. The start of the higher order pattern is visible on the right. Spectrum has been fitted with fourteen Lorentzian profiles.

5.2. Zeeman Effect in 5460Å

A typical fitted spectrum is shown in Figure 4. This is the $6^3S_1 \rightarrow 7^3P_2$ transition, with g-factors 2 and 3/2, respectively. Following discussion in Section 2, we expect nine peaks evenly spaced by an energy separation $\Delta E = \hbar eB/4m_e$. We plot the off-center displacement of the eight outside peaks against magnetic field in Figure 5. The linear fits pictured had χ^2_ν values ranging from 0.5 to 5. The *wavenumber separation* $\Delta\,(1/\lambda)$ of a peak from its neighbor is related to the fundamental quantity e/m.

$$\Delta\left(\frac{1}{\lambda}\right) = \frac{B}{8\pi c}\left(\frac{e}{m_e}\right) \tag{6}$$

Using the established value of c, the eight lines give a result of $e/m = 1.82(4) \times 10^{11}$ C/kg. The accepted NIST value is 1.76×10^{11} C/kg.

5.3. Zeeman Effect in 5770Åand 5790Å

Our investigation of this line was unsuccessful. The off-center displacement of the left and right peaks of the 5770Å and 5790Å lines are plotted against magnetic field in Figure 6.

The 5790Å transition is $^1D_2 \rightarrow ^1P_1$, with no change in g-factor. The wavenumber separation $\Delta\,(1/\lambda)$ is twice

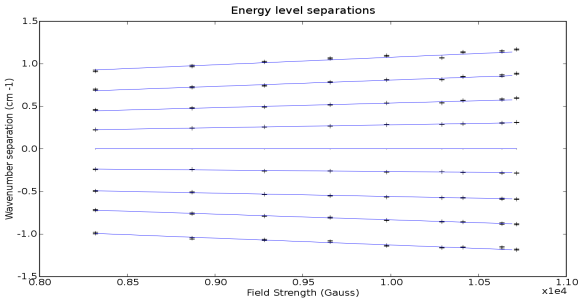

FIG. 5: Off-center displacement in wavenumbers of the eight outside peaks in the green line of mercury as a function of magnetic field strength.

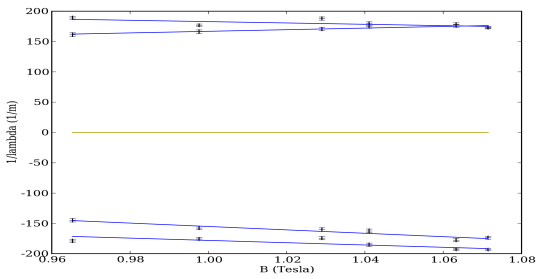

FIG. 6: Off-center displacement in wavenumbers of the four outside peaks in the yellow doublet of mercury as a function of magnetic field strength. Top to bottom, they are the right peak of the 5770Å line, the right peak of the 5790Å line, the left peak of the 5790Å line and the left peak of the 5790Å line.

that of what it was in Equation 6. Linear fits were performed with reduced-chi-squared parameters of 2.1 and 1.2. The two lines give a result of $e/m = 7.7(8) \times 10^{11}$ C/kg. We will discuss the causes for this outlier shortly.

The 5770Å transition is ${}^3D_2 \rightarrow {}^1P_1$, moving from a g-factor of 7/6 to 1. Thus, we expect three main lines, each splitting slightly into three separate lines. Since we do not expect to be able to resolve the finer splitting, we simply treat this transition as if it only had three peaks. Unfortunately, these peaks appear to be moving in the same direction relative to the center peak and the linear fits have $\chi^2_\nu = 5.4$ and 6.3. Thus, we do not attempt derive the value e/m using this data.

6. CONCLUSION

We have qualitatively confirmed hyperfine structure in the 5460Å ${}^3S_1 \rightarrow {}^3P_2$ transition of mercury. The extraordinary width of the unresolved central peak is due to the splitting between even isotopes caused by the mass and volume effect. The left and right peaks are due to the presence of the odd isotopes of mercury. However, the calculated energy offsets are too high by on the order of 10%. Though this could be caused by a systematic energy miscalibration, this possibility seems unlikely in light of the next set of results. We have no immediate and satisfying explanation for the discrepancy.

We have quantitatively confirmed the Zeeman effect in this same transition, namely, the linear dependence of energy shift with magnetic field, the theoretical value of the g-factor, and the ratio of the electron charge to mass. Our value, $e/m = 1.82(4) \times 10^{11}$ C/kg is in excellent agreement with the accepted value, and is within one and a half standard deviations.

Due to a number of factors, we were not able to confirm the Zeeman effect in the 5770Å and 5790Å doublet in mercury. The fundamental issue is one of resolution. When all three relatively wide peaks have a separation of less than ten bins, resolution is challenging. The width of the peaks came from several sources, including Doppler broadening, spectrum smearing due to large aperture size, and the effect of the Fabry-Perot apparatus on lineshape.

Additionally, the choice of free spectral range was constrained by two factors: we required that it be large enough to contain another order of the transition line, but low enough to clearly resolve the Zeeman splitting at high fields. In attempting to accomplish the former goal, we have compromised the latter. Finally, our choice of fitting method further mangled attempts to obtain reasonable data. If the true lineshape is relatively Gaussian, fitting to a Lorentzian profile will cause the fitting algorithm to overcompensate for the tall "tails" of the latter and attempt to move groups of peaks closer to each other to minimize the amount of tail that contributes to the background.

Our results are mixed. Only our investigation of the green line of mercury can be said to be successful. Our investigation of the yellow doublet is inconclusive, and a candidate for careful repetition.

[1] URL `http://hyperphysics.phy-astr.gsu.edu/`.
[2] J. L. Staff, *Zeeman effect and hyperfine structure in mercury*, URL `http://web.mit.edu/8.13/www/JLExperiments/JLExp06.pdf`.
[3] P. Bevington and D. Robinson, *Data Reduction and Error Analysis for the Physical Sciences* (McGraw-Hill, 2003).
[4] Journal of Physics B **3** (1970).

Acknowledgments

DVP gratefully acknowledges Brian Pepper's equal partnership, as well as the guidance and advice of Thomas Walker, Daniel Nezich and Scott Sewell.